Journal of the Korean Physical Society (2024) 84:151–157
https://doi.org/10.1007/s40042-023-00987-4

Online ISSN 1976-8524
Print ISSN 0374-4884

ORIGINAL PAPER - CONDENSED MATTER

Random-singlet-like state emergent in $s = 5/2$ frustrated cubic lattice

Chanhyeon Lee[1] · Sang-Kwon Lee[1] · Suheon Lee[2] · J. van Tol[3] · Kwang-Yong Choi[4]

Received: 12 October 2023 / Revised: 2 November 2023 / Accepted: 17 November 2023 / Published online: 3 January 2024

Abstract

We employ thermodynamic and electron spin resonance (ESR) techniques to elucidate the effects of quenched disorder on a ground state of $s = 5/2$ frustrated cubic antiferromagnet $La_3Sb_3Mn_2O_{14}$. We observe the development of multiple ESR lines for temperatures below 80 K. Concomitantly, the ESR linewidth exhibits a power-law increase, accompanied by an intriguing shift in resonance fields. These observations point to the occurrence of inhomogeneous magnetism. Additionally, *ac* magnetic susceptibility and magnetization data obey a scaling relation of $\chi'(H, T)$ and $M(H, T)$ in $\mu_B H/k_B T$ with the scaling exponent $\alpha = 0.53$. This scaling behavior alludes to the formation of a random-singlet-like state and the presence of abundant low-lying excitations. Our results highlight the concerted interplay of strong disorder and frustration to stabilize a putative random-singlet state even in classical and high-dimensional spin systems.

Keywords Quantum magnet · Random singlet · Quantum scalings · Frustration

1 Introduction

Geometrically frustrated spin systems have emerged as fertile grounds for exploring novel phases of matter and unraveling the intricate interplay of quantum many-body states, frustration, and disorder [1–7]. Frustration originates from geometric constraints imposed by the lattice structure, where triangular, tetrahedral, or Kagome motifs can prohibit conventional magnetic order. Rather, frustrated magnetic systems often give rise to unconventional ground states such as spin liquids and spin ice [8].

One particularly intriguing aspect of frustrated spin systems is the appearance of random singlets instead of conventional spin glass or sought-after quantum spin liquids when quenched disorder or randomness is introduced [9–19]. The random-singlet state comprises a minor fraction of intrinsic orphan spins and a major fraction of singlet clusters, leading to a power-law distribution of exchange energies and density of states $N(E) \sim E^{-\alpha}$ [20–23]. The signature of random singlets manifests in the power-law dependencies of various thermodynamic quantities, such as specific heat, magnetic susceptibility, and thermal conductivity and their unconventional scaling behavior.

Notably, quantum spin liquids and random singlets commonly share the absence of conventional magnetic order and fractionalized excitations. However, they show disparities in their mechanisms, symmetries, and the presence of topological order. Quantum spin liquids induced by quantum fluctuations entail emergent gauge symmetries and topological order while retaining global symmetries. In contrast, the disorder-induced random singlets break a translational symmetry and typically lack topological order. In this light, a study of random singlets advances our understanding of quantum phases in spin systems, offering unique insights into the behavior of matter in the presence of disorder and frustration.

Beyond the phenomenological description, it is highly controversial whether random singlets are stabilized in high-dimensional frustrated magnets [12–18, 21, 22]. On the experimental front, several random-singlet candidate materials have been reported. The representative instances include, triangular antiferromagnet $YbMgGaO_4$ with antisite

✉ Kwang-Yong Choi
choisky99@skku.edu

[1] Department of Physics, Chung-Ang University, Seoul 06974, Republic of Korea

[2] Center for Artificial Low Dimensional Electronic Systems, Institute for Basic Science (IBS), Pohang 37673, Republic of Korea

[3] National High Magnetic Field Laboratory, Florida State University, Tallahassee, FL 32310-3706, USA

[4] Department of Physics, Sungkyunkwan University, Suwon 16419, Republic of Korea

mixing between nonmagnetic Mg^{2+} and Ga^{3+} ions [21], square compound $Sr_2CuTe_{1-x}W_xO_6$ with W-for-Te substitution [24–28], Kitaev honeycomb lattices Cu_2IrO_3, $H_3LiIr_2O_6$, and α-$Ru_{1-x}Ir_xCl_3$ [29–32]. Very recently, the purview of random-singlet physics has been extended to three-dimensional (3D) frustrated cubic lattice $Lu_3Sb_3Mn_2O_{14}$ with a $s = 5/2$ spin number [33]. As sketched in Fig. 1a–c, a family of $RE_3Sb_3Mn_2O_{14}$ (RE=rare earth) constitutes a 3D Shastry–Sutherland-like model that is a cubic lattice with face diagonal interactions. Thus, further experimental investigations of $RE_3Sb_3Mn_2O_{14}$ enable deepening our understanding of the conditions under which random singlets can be stable in high-dimensional frustrated magnets.

In this paper, we investigate random-singlet characteristics in $La_3Sb_3Mn_2O_{14}$, which is isostructural to $s = 5/2$ 3D frustrated cubic antiferromagnet $Lu_3Sb_3Mn_2O_{14}$. We identify the temperature and field scalings of *ac* magnetic susceptibility and magnetization with complementary exponent, indicative of a random-singlet scenario. Our results suggest that a random-singlet state might be viable even for 3D classical frustrated antiferromagnets.

2 Experimental details

Polycrystalline samples of $La_3Sb_3Mn_2O_{14}$ were prepared by the conventional solid-state reaction method. Stoichiometric amounts of La_2O_3, Sb_2O_5, and $MnCO_3$ were ground and then calcinated at 850°C for 12 h. Subsequently, the mixture was sintered at 1200°C for 48 h. To assess the phase purity of the obtained samples, a powder X-ray diffraction (XRD) analysis was conducted at room temperature using Cu-Kα radiation. We made a refined analysis of the XRD pattern using the Fullprof program, as shown in Fig. 1d. The lattice parameters determined from the Rietveld refinements are $a = b = 7.55522$ Å and $c = 17.80629$ Å. We summarize the atomic coordinates with Wyckoff positions in Table 1 with the goodness of fit $R_p = 3.24\%$ and $R_{wp} = 4.12\%$.

dc and *ac* magnetic susceptibilities and isothermal magnetization were measured using a VSM-SQUID (superconducting quantum interference device) magnetometer (MPMS3, Quantum Design) at the Center for Condensed Matter Science, NTU. The temperature-dependent *dc* magnetic susceptibility was measured in a range of $2 - 300$ K by applying an external magnetic field of 1 T. Isothermal magnetization curves were recorded at selected temperatures $T = 2, 3, 4, 5, 8, 12$, and 20 K with magnetic fields ranging from 0 to 14 T. For *ac* magnetic susceptibility measurements, we used an oscillating field of 5 Oe at frequencies $\nu = 2 - 100$ Hz under a zero-*dc* field condition. We measured field- and temperature-dependent *ac* susceptibility by selecting various applied magnetic fields $\mu_0 H = 0.1, 1, 2, 3, 5$, and 7 T at a fixed frequency of $\nu = 100$ Hz. High-field ESR experiments were performed with a heterodyne spectrometer

Table 1 Atomic positions of $La_3Sb_3Mn_2O_{14}$ obtained from the Rietveld refinement in the $R\bar{3}m$ space group

Atom	Wyckoff site	x	y	z
Mn1	3a	0	0	0
Mn2	3b	0	0	1/2
Sb	9d	1/2	0	1/2
La	9e	1/2	0	0
O1	6c	0	0	0.3836(9))
O2	18h	0.5312(9)	−0.5312(9)	0.1478(9)
O3	18h	0.1405(9)	−0.1405(9)	−0.0574(1)

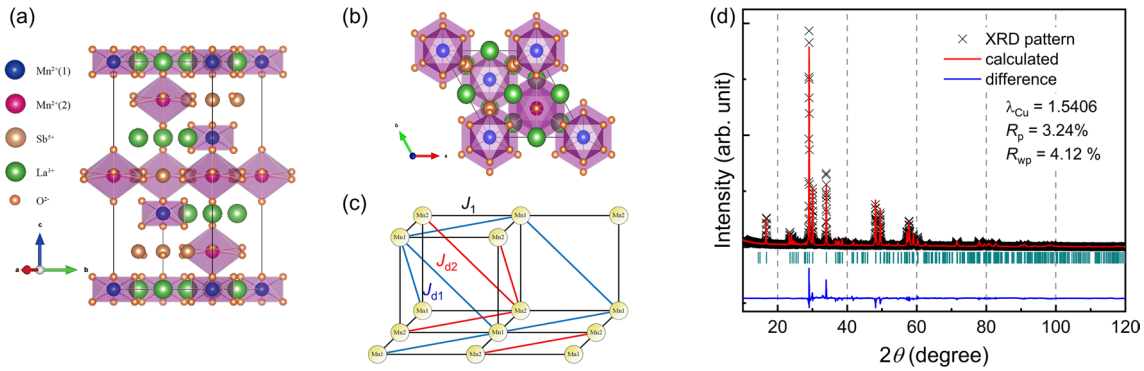

Fig. 1 **a** Crystal structure of $La_3Sb_3Mn_2O_{14}$. The red and blue balls represent Mn(1) and Mn(2), and the orange balls stand for O atoms. The La and Sb atoms are depicted by the green and brown balls. **b** Projection of the crystal structure onto the *ab* plane. The Mn^{2+} ions possess two different magnetic environments: $Mn(1)O_8$ hexagonal bipyramids and $Mn(2)O_6$ octahedra. **c** Frustrated magnetic model of $La_3Sb_3Mn_2O_{14}$ consisting of an edge coupling J_1 (black line) and two different face diagonal interactions J_{d1} (blue line) and J_{d2} (red line). **d** Rietveld refinement of the XRD diffraction pattern of $La_3Sb_3Mn_2O_{14}$. The black cross, the red solid line, the blue line, and the green vertical dashed lines are the XRD, calculated, difference curve, and Bragg peaks, respectively

at a fixed frequency $\nu = 240$ GHz at National High Magnetic Field Laboratory in Tallahassee, Florida, USA. The temperature is varied from $T = 2$ K to 200 K using a liquid helium cryostat.

3 Results and discussion

3.1 Spin topology and magnetic properties

Figure 1a shows the crystal structure of $La_3Sb_3Mn_2O_{14}$, in which Mn^{2+} triangular layers are sandwiched between alternating La and Sb Kagome layers. The crystal structure features two distinct crystallographic sites for Mn(1) and Mn(2) ions; Mn(1) atoms are coordinated by $Mn(1)O_8$ hexagonal bipyramids, while Mn(2) atoms are surrounded by Mn(2) O_6 octahedra. Notably, Mn–O–Mn superexchange paths are lacking since the Mn^{2+} ions between metal-oxygen polyhedra are not linked through O^{2-} ions (see Fig. 1b). Consequently, the spin topology is determined by Mn–O–O–Mn super–super exchange paths, resulting in a frustrated cubic lattice including three main interactions: (i) the nearest-neighbor Mn(1)-Mn(2) interaction J_1 (black line in Fig. 1c), (ii) the next-nearest neighbor Mn(1)- Mn(1) interaction J_{d1} (blue line), and (iii) Mn(2)-Mn(2) interaction J_{d2} (red line).

Figure 2a presents the temperature-dependent magnetic susceptibility $\chi(T)$ measured under an external magnetic field of $\mu_0 H = 1$ T. As the temperature is cooled down to 2 K, $\chi(T)$ steeply increases with no appreciable difference between the zero-field-cooled (ZFC) and field-cooled (FC) data. This observation rules out the occurrence of long-range magnetic ordering or spin freezing. Moreover, the absence of spin-glass transition is corroborated by the in-phase component of the *ac* susceptibility $\chi'(T)$, which reveals no discernible frequency dependence (see Fig. 2b). In Fig. 2c, we plot the temperature dependence of $1/\chi(T)$. We could identify a two-stage Curie–Weiss behavior. In the high-temperature regime above 140 K, the Curie–Weiss fit yields the Curie–Weiss temperature $\Theta_{CW}^{H} = 61.9(7)$ K and the effective magnetic moment $\mu_{eff}^{H} = 3.77\ \mu_B$. Conversely, in the low-temperature range of $T = 20 - 130$ K, the Curie–Weiss temperature is reduced to $\Theta_{CW}^{L} = -19.2(2)$ K with a change in sign. Furthermore, the effective magnetic moment $\mu_{eff}^{L} = 5.71\ \mu_B$ becomes comparable to the theoretical spin-only value of $\mu_{eff}^{theo} = 5.82\ \mu_B$ with the *g*-factor of $g = 1.99$, as evaluated through electron spin resonance in Fig. 3a. This intriguing two-stage Curie–Weiss behavior is often linked to the complexity of magnetic interactions. Since the studied compound lacks structural instabilities, diverse exchange interactions, differing in sign and strength, come into

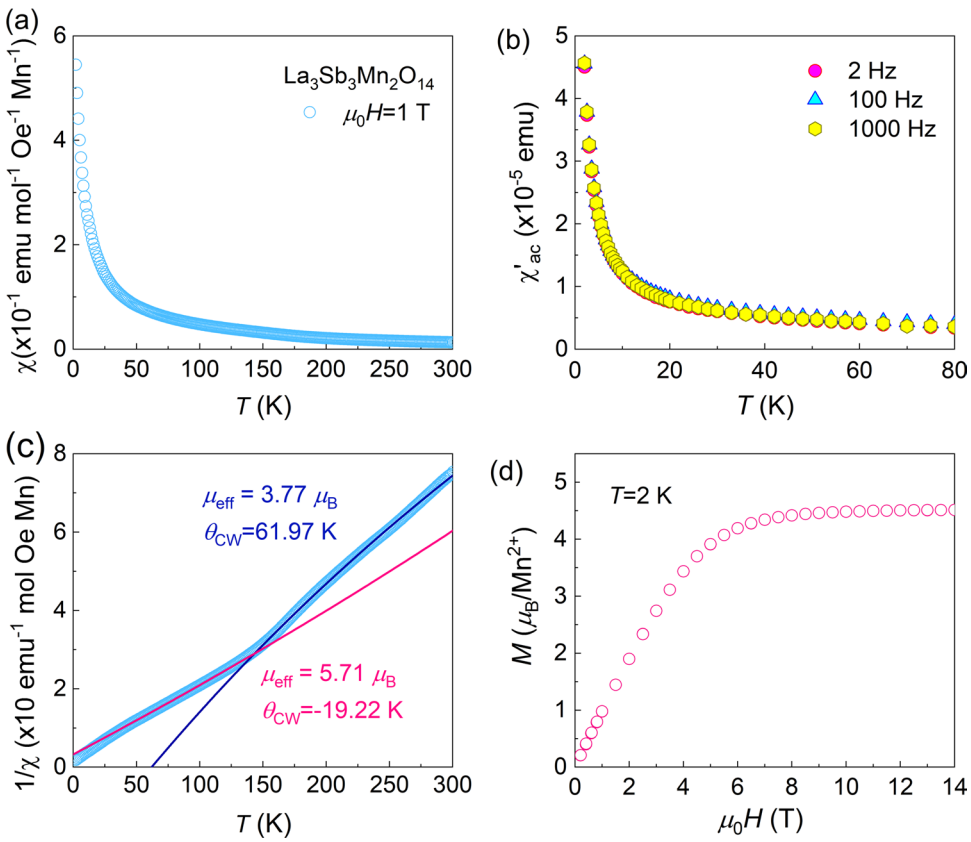

Fig. 2 **a** Temperature dependence of the *dc* magnetic susceptibility of $La_3Sb_3Mn_2O_{14}$ in an external magnetic field of 1 T. **b** Temperature dependence of *ac* magnetic susceptibility measured at selected frequencies $\nu = 2$, 100, and 1000 Hz. **c** Inverse susceptibility data versus temperature. The solid lines denote Curie–Weiss fits at two different temperature regimes. **d** Isothermal magnetization curve measured at $T = 2$ K

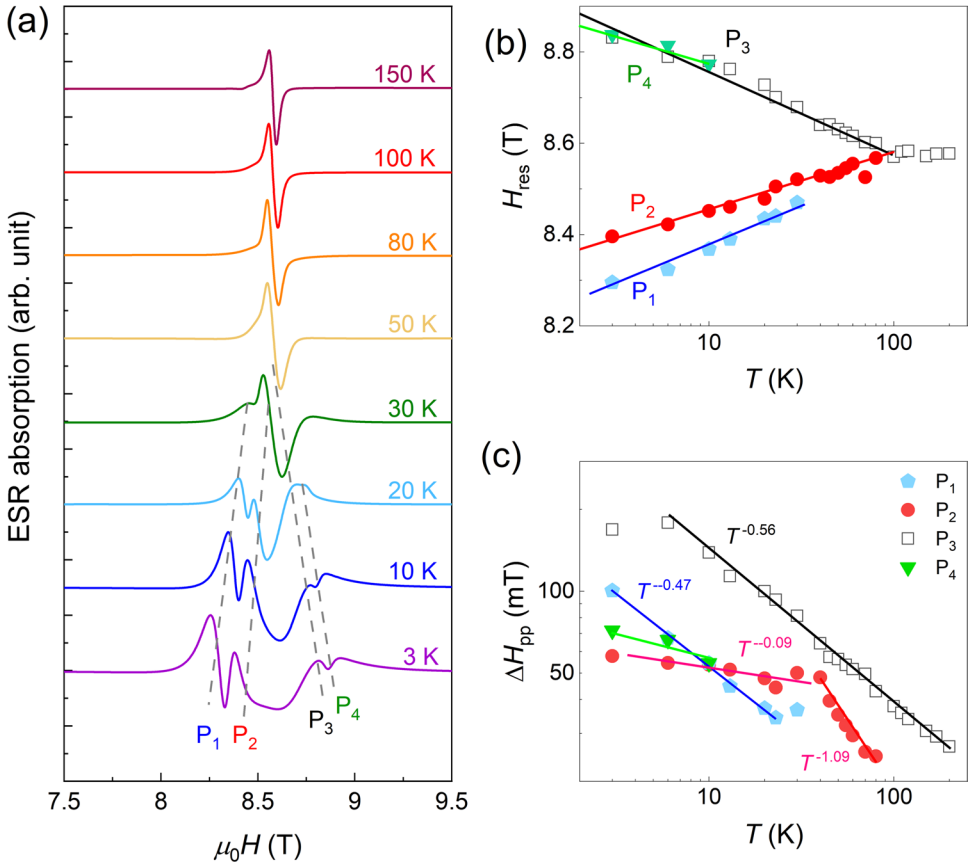

Fig. 3 **a** Temperature dependence of the high-frequency ESR spectrum measured at $\nu = 240$ Hz. The dashed lines are a guide to the eye. **b** Resonance field versus temperature. **c** Temperature dependence of peak-to-peak width. The solid lines are power-law behaviors

play, exerting their influence on the magnetic properties at different temperature ranges. In our case, J_1 is antiferromagnetic while J_{d1} and J_{d2} tend to exhibit ferromagnetic tendencies [34].

In Fig. 2d, we present the magnetization curve $M(H)$ recorded at $T = 2$ K. With increasing field, $M(H)$ shows a linear-like increase, followed by saturation at $M_S = gS\mu_B \approx 4.51\ \mu_B$ at the saturation field $\mu_0 H_S \approx 6$ T. $\mu_0 H_S$ turns out to be considerably smaller than the energy scale of $|\Theta_{CW}| = 19.22$ K, possibly implying that subdominant ferromagnetic interactions are present in addition to the leading antiferromagnetic interaction between Mn^{2+} spins [34]. Eventually, the magnetization may attain the expected saturation value of approximately 4.97 μ_B. Compared to $La_3Sb_3Mn_2O_{14}$, the isostructural compound $Lu_3Sb_3Mn_2O_{14}$ exhibits a higher saturation field $\mu_0 H_S^{Lu}$ at approximately 45 T and a larger Curie–Weiss temperature Θ_{CW}^{Lu} at −43.48 K, and a saturation magnetization of 4.93 μ_B [33]. This contrast indicates that the antiferromagnetic interactions become weaker relative to the ferromagnetic interactions by replacing Lu with La, highlighting the sensitivity of the magnetic interactions to the constituent RE element.

3.2 Electron spin resonance

To gain insight into the evolution of spin correlations, we employ a local dynamical probe of spin fluctuations. Figure 3a plots the temperature dependence of high-frequency ESR signals. At elevated temperatures, the ESR signal features a single Lorentzian profile. With decreasing temperature through 80 K, additional ESR signals start to emerge, resulting in four distinct signals at $T = 3$ K. For a quantitative analysis, we fit the ESR spectra to a sum of four powder-averaged Lorentzian profiles. The extracted resonance field $H_{res}(T)$ and the peak-to-peak linewidth $\Delta H_{pp}(T)$ are exhibited in Figs. 3b, c, respectively.

Upon cooling from 80 K, $H_{res}(T)$ for the P1 and P2 absorption lines shift toward lower fields, while those for the P3 and P4 lines shift in the opposite direction, toward higher field. Since the resonance field reflects the development of internal magnetic fields, the multiple ESR lines with oppositive evolution of $H_{res}(T)$ imply the existence of spatially inhomogeneous magnetic correlations. Specifically, a fraction of spins is engaged in ferromagnetic correlations, while others develop antiferromagnetic correlations. In addition, each absorption line obeys a critical power-law

dependence $\Delta H_{pp}(T) \sim T^{-\alpha}$ with the exponents of $\alpha = 0.47$ in the $T = 3 - 35$ K for P1, $\alpha = 0.56$ in the $T = 3 - 150$ K for P3, and the changing exponent from $\alpha = 1.09$ to 0.09 through 40 K for P2. We note that the critical-like line broadening may be associated with the development of critical magnetic correlations or spatially random local fields. We recall that triangular antiferromagnet $Ba_3CuSb_2O_9$ with Cu^{2+}/Sb^{5+} disorders shows the critical ESR line broadening that is taken as a sign of a random-singlet state [35]. In this vein, the switching power-law dependence of $\Delta H_{pp}(T)$ for P2 is attributed to variations in both defects and the strength of magnetic interactions, which give rise to the development of distinct magnetic correlations through 40 K.

3.3 Quantum scalings of magnetization and magnetic susceptibility

To examine a random-singlet scenario hinted by the high-frequency ESR data, we collected the *ac* magnetic susceptibility and magnetization in a two-dimensional parameter space of temperature and magnetic field.

Figure 4a exhibits the H and T dependencies of $\chi'(H, T)$ measured at a fixed frequency $\nu = 100$ Hz in various *dc* fields of $\mu_0 H = 0.1 - 7$ T. The log–log plot of $\chi'(\mu_0 H = 0.1\ \text{T}, T)$ reveals a sub-Curie behavior of $T^{-0.53}$ in the wide temperature range of $T = 7 - 80$ K, which is often taken as evidence of random magnetism. With increasing field, $\chi'(H, T < 25\ \text{K})$ is systematically suppressed as an external magnetic field engenders the freezing of weakly coupled spins. Eventually, the broad $T = 20$ K maximum becomes discernible for $\chi'(\mu_0 H = 7\ \text{T}, T)$. By plotting $T^{\alpha}\chi'$ versus $\mu_B H/k_B T$ in Fig. 4b, the $\chi'(H, T)$ data fall onto a single curve with the scaling exponent $\alpha = 0.53$ over nearly three orders of magnitude. Figure 4c shows the temperature dependence of the magnetization curves $M(H, T)$. In Fig. 4d, we plot $MT^{0.47}$ against the dimensionless variable $\mu_B H/k_B T$, confirming the data collapse over almost three orders of magnitude. We note that the scaling exponents deduced from $\chi'(H, T)$ and $M(H, T)$ are complimentary. This means that the $T - H$ scalings of $\chi'(H, T)$ and $M(H, T)$ are rooted in the same divergent power-law DOS of $N(E) \sim E^{-\alpha}$ ($\alpha \approx 0.53$). We note that the divergent power-law DOS gives rise to the power-law behaviors of $\chi \sim T^{-\alpha}$, $M \sim H^{1-\alpha}$, and $C_m \sim T^{1-\alpha}$ (see Table II in Ref. [22]). Furthermore, we stress that the sister compound $Lu_3Sb_3Mn_2O_{14}$ shows the similar scaling relation with $\alpha^{Lu} \approx 0.78$ [33]. The scaling exponent is not universal, depending roughly on the degree of quenched disorder. In the studied compound, quenched disorders are generated by Mn(1)/Mn(2) defects or vacancies as well as antisite mixing between Mn(1)/La and Mn(2)/Sb [36]. The Mn(1)/Mn(2) vacancies disrupt the 3D frustrated spin network consisting of $J_1 - J_{d1} - J_{d2}$, leading to exchange randomness among the three distinct interactions (see Fig. 1c). Since the exchange interactions have different signs, both ferromagnetic and antiferromagnetic correlations can develop as evinced by the high-frequency ESR data [34].

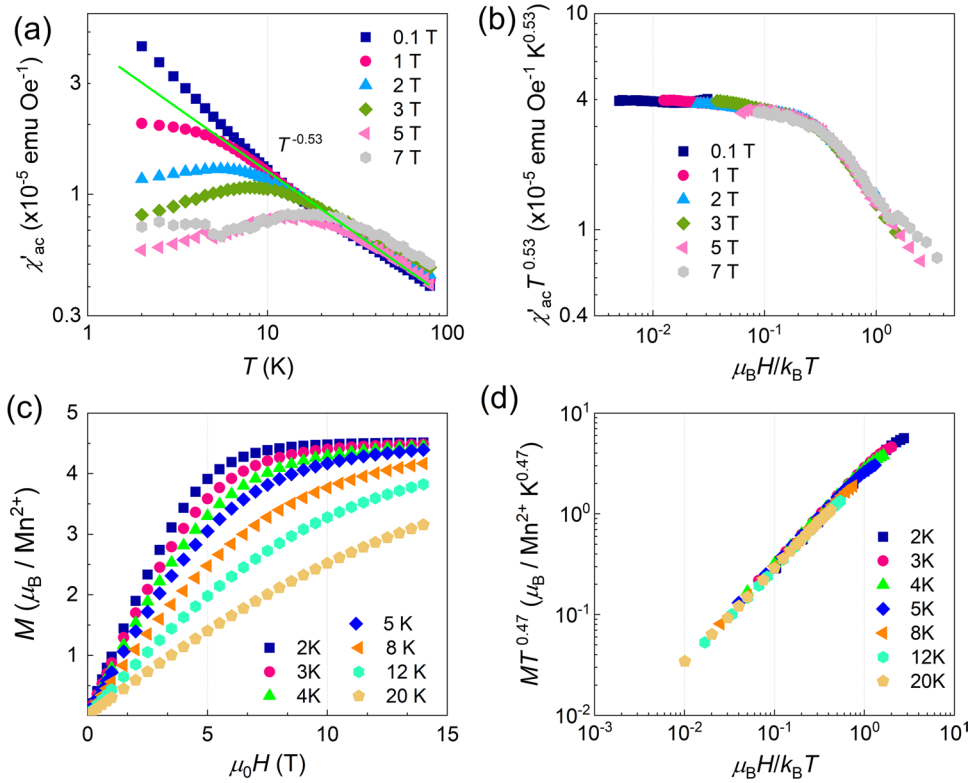

Fig. 4 **a** Temperature and field dependence of $\chi'(T)$ measured at $\nu = 100$ Hz and an oscillating field 10 Oe. The green line denotes a $T^{-0.53}$ dependence. **b** Scaling of $\chi' T^{0.53}$ versus $\mu_B H/k_B T$ on a log-log scale. **c** Magnetization curves $M(H)$ at selected temperatures ranging from $T = 2$ K to 20 K. **d** Double logarithmic scaled plot of $MT^{0.47}$ versus $\mu_B H/k_B T$

Our findings suggest that a random-singlet state can persist in spite of large spin number and 3D spin network.

4 Conclusions

In conclusion, we have conducted thermodynamic and electron spin resonance measurements of $La_3Sb_3Mn_2O_{14}$. Our ESR data reveal the simultaneous shift of the resonance field and the power-law increase of the ESR linewidth, indicative of the existence of an inhomogeneous magnetic state as a consequence of quenched disorder. Furthermore, we find scaling collapses of the magnetic-field- and temperature-dependent $\chi'(H, T)$ and $M(H, T)$, being consistent with a random-singlet scenario. The exponent $\alpha = 0.53$ extracted from the power-law behaviors signifies the abundance of low-energy power-law density of states. The putative random singlet suggests that the confluence of strong disorder and frustration can stabilize a random-singlet state even in classical and high-dimensional spin systems.

Acknowledgements CHL was supported by the Chung-Ang University Excellent Student Scholarship in 2019. The National High Magnetic Field Laboratory is supported by the National Science Foundation through Grant No. NSF/DMR-1644779 and the State of Florida.

References

1. Y. Zhou, K. Kanoda, T.-K. Ng, Quantum spin liquid states. Rev. Mod. Phys. **89**, 025003 (2017)
2. D. Wulferding, Y. Choi, W. Lee, K.-Y. Choi, Raman spectroscopic diagnostic of quantum spin liquids. J. Phys.: Condens. Matter **32**, 043001 (2020)
3. Z.H. Jang, Investigation of the metallic property of noble metal nanoparticles with 1H solid-state NMR. J. Korean Phys. Soc. **81**, 428–433 (2022)
4. C.J. Kang, J. Hong, J. Kim, Dynamical mean-field theory study of a ferromagnetic CrI3 monolayer. J. Korean Phys. Soc. **80**, 1071–1075 (2022)
5. S.Y. Kim, Study of the frustrated Ising model on a square lattice based on the exact density of states. J. Korean Phys. Soc. **79**, 894–902 (2021)
6. J.H. Lee, H.C. Lee, Machine learning study of the deformed one-dimensional topological superconductor. J. Korean Phys. Soc. **79**, 173–184 (2021)
7. M. Ancliff, V. Sachnev, Numerical estimation of the ground states of frustrated antiferromagnet gadolinium gallium garnet. J. Korean Phys. Soc. **82**, 699–706 (2023)
8. C. Castelnovo, R. Moessner, S.L. Sondhi, Magnetic monopoles in spin ice. Nature **451**, 42 (2008)
9. J. Oitmaa, O.P. Sushkov, Two-Dimensional randomly frustrated spin-1/2 heisenberg model. Phys. Rev. Lett. **87**, 167206 (2001)
10. Y.-C. Lin, H. Rieger, N. Laflorencie, F. Iglói, Strong-disorder renormalization group study of $S = 1/2$ Heisenberg antiferromagnet layers and bilayers with bond randomness, site dilution, and dimer dilution. Phys. Rev. B **74**, 024427 (2006)
11. R.R.P. Singh, Valence bond glass phase in dilute kagome antiferromagnets. Phys. Rev. Lett. **104**, 177203 (2010)
12. K. Watanabe, H. Kawamura, H. Nakano, T. Sakai, Quantum spin-liquid behavior in the spin-1/2 random Heisenberg antiferromagnet on the triangular lattice. J. Phys. Soc. Jpn. **83**, 034714 (2014)
13. H. Kawamura, K. Watanabe, T. Shimokawa, Quantum spin-liquid behavior in the spin-1/2 random-bond Heisenberg antiferromagnet on the kagome lattice. J. Phys. Soc. Jpn. **83**, 103704 (2014)
14. T. Shimokawa, K. Watanabe, H. Kawamura, Static and dynamical spin correlations of the S=1/2 random-bond antiferromagnetic Heisenberg model on the triangular and kagome lattices. Phys. Rev. B **92**, 134407 (2015)
15. L. Liu, H. Shao, Y.-C. Lin, W. Guo, A.W. Sandvik, Random-singlet phase in disordered two-dimensional quantum magnets. Phys. Rev. X **8**, 041040 (2018)
16. K. Uematsu, H. Kawamura, Randomness-induced quantum spin liquid behavior in the s=1 random J1–J2 Heisenberg antiferromagnet on the square lattice. Phys. Rev. B **98**, 134427 (2018)
17. H.-Q. Wu, S.-S. Gong, D.N. Sheng, Randomness-induced spin-liquid-like phase in the spin-1/2 J1–J2 triangular Heisenberg model. Phys. Rev. B **99**, 085141 (2019)
18. K. Uematsu, H. Kawamura, Randomness-induced quantum spin liquid behavior in the S=1/2 random-bond Heisenberg antiferromagnet on the pyrochlore lattice. Phys. Rev. Lett. **123**, 087201 (2019)
19. H. Kawamura, K. Uematsu, Nature of the randomness-induced quantum spin liquids in two dimensions. J. Phys. Condens. Matter **31**, 504003 (2019)
20. R.N. Bhatt, P.A. Lee, Scaling studies of highly disordered antiferromagnetic systems. Phys. Rev. Lett. **48**, 344 (1982)
21. I. Kimchi, J.P. Sheckelton, T.M. McQueen, P.A. Lee, Scaling and data collapse from local moments in frustrated disordered quantum spin systems. Nat. Commun. **9**, 4367 (2018)
22. I. Kimchi, A. Nahum, T. Senthil, Valence bonds in random quantum magnets: theory and application to $YbMgGaO_4$. Phys. Rev. X **8**, 031028 (2018)
23. L. Liu, W. Guo, A.W. Sandvik, Quantum-critical scaling properties of the two-dimensional random-singlet state. Phys. Rev. B **102**, 054443 (2020)
24. O. Mustonen, S. Vasala, E. Sadrollahi, K.P. Schmidt, C. Baines, H.C. Walker, I. Terasaki, F.J. Litterst, E. Baggio-Saitovitch, M. Karppinen, Spin-liquid-like state in a spin-1/2 square-lattice antiferromagnet perovskite induced by d10/d0 cation mixing. Nat. Commun. **9**, 1085 (2016)
25. O. Mustonen, S. Vasala, K.P. Schmidt, E. Sadrollahi, H.C. Walker, I. Terasaki, F.J. Litterst, E. Baggio-Saitovitch, M. Karppinen, Tuning the S=1/2 square-lattice antiferromagnet Sr2Cu(Te1-xWx) O6 from Néel order to quantum disorder to columnar order. Phys. Rev. B **98**, 064411 (2018)
26. W. Hong, L. Liu, C. Liu, X. Ma, A. Koda, X. Li, J. Song, W. Yang, J. Yang, P. Cheng, H. Zhang, W. Bao, X. Ma, D. Chen, K. Sun, W. Guo, H. Luo, A.W. Sandvik, S. Li, Extreme suppression of antiferromagnetic order and critical scaling in a two-dimensional random quantum magnet. Phys. Rev. Lett. **126**, 037201 (2021)
27. S. Yoon, W. Lee, S. Lee, J. Park, C.H. Lee, Y.S. Choi, S.-H. Do, W.-J. Choi, W.-T. Chen, F. Chou, D.I. Gorbunov, Y. Oshima, A. Ali, Y. Singh, A. Berlie, I. Watanabe, K.-Y. Choi, Quantum disordered state in the J1–J2 square-lattice antiferromagnet $Sr_2Cu(Te_{0.95}W_{0.05})O_6$. Phys. Rev. Mater. **5**, 014411 (2021)
28. H.-D. Ren, T.-Y. Xiong, H.-Q. Wu, D.N. Sheng, S.-S. Gong, Characterizing random-singlet state in two-dimensional frustrated quantum magnets and implications for the double perovskite SrCuTe1-xWxO6. Phys. Rev. B **107**, L020407 (2023)
29. Y.S. Choi, C.H. Lee, S. Lee, S. Yoon, W.-J. Lee, J. Park, A. Ali, Y. Singh, J.-C. Orain, G. Kim, J.-S. Rhyee, W.-T. Chen, F. Chou, K.-Y. Choi, Exotic low-energy excitations emergent in the random kitaev magnet Cu_2IrO_3. Phys. Rev. Lett. **122**, 167202 (2019)

30. S.-H. Do, C.H. Lee, T. Kihara, Y.S. Choi, S. Yoon, K. Kim, H. Cheong, W.-T. Chen, F. Chou, H. Nojiri, K.-Y. Choi, Randomly hopping Majorana fermions in the diluted Kitaev system α-$Ru_{0.8}Ir_{0.2}Cl_3$. Phys. Rev. Lett. **124**, 047204 (2020)
31. S.-H. Baek, H.W. Yeo, S.-H. Do, K.-Y. Choi, L. Janssen, M. Vojta, B. Büchner, Observation of a random singlet state in a diluted Kitaev honeycomb material. Phys. Rev. B **102**, 094407 (2020)
32. C. Lee, S. Lee, Y. Choi, C. Wang, H. Luetkens, T. Shiroka, Z.H. Jang, Y.-G. Yoon, K.-Y. Choi, Coexistence of random singlets and disordered Kitaev spin liquid in H3LiIr2O6. Phys. Rev. B **107**, 014424 (2023)
33. C. Lee, S. Lee, H.-S. Kim, S. Kittaka, Y. Kohama, T. Sakakibara, K.H. Lee, J. van Tol, D.I. Gorbunov, S.-H. Do, S. Yoon, A. Berlie, K.-Y. Choi, Phys. Rev. B **107**, 214404 (2023)
34. Private communication with Heungsik Kim provided preliminary DFT calculation results on exchange interactions on $RE_3Sb_3Mn_2O_{14}$
35. S.-H. Do, J. van Tol, H.D. Zhou, K.-Y. Choi, Dynamical spin-orbital correlations versus random singlets in $Ba_3CuSb_2O_9$ investigated by magnetization and electron spin resonance. Phys. Rev. B **90**, 104426 (2014)
36. W.T. Fu, D.J.W. IJdo, Crystal structure of $Mn_2Ln_3Sb_3O_{14}$ (Ln=La, Pr and Nd): A new ordered rhombohedral pyrochlore. J. Solid State Chem. **213**, 65 (2014)